

## Calculation of Voltage Stability Margins and Certification of Power Flow Insolvability using Second-Order Cone Programming

Daniel K. Molzahn  
University of Michigan  
molzahn@umich.edu

Ian A. Hiskens  
University of Michigan  
hiskens@umich.edu

Bernard C. Lesieutre  
University of Wisconsin–Madison  
lesieutre@wisc.edu

### Abstract

*Reliable power system operation requires maintaining sufficient voltage stability margins. Traditional techniques based on continuation and optimization calculate lower bounds for these margins and generally require appropriate initialization. Building on a previous semidefinite programming (SDP) formulation, this paper proposes a new second-order cone programming (SOCP) formulation which directly yields upper bounds for the voltage stability margin without needing to specify an initialization. Augmentation with integer-constrained variables enables consideration of reactive-power-limited generators. Further, leveraging the ability to globally solve these problems, this paper describes a sufficient condition for insolvability of the power flow equations. Trade-offs between tightness and computational speed of the SDP and SOCP relaxations are studied using large test cases representing portions of European power systems.*

### 1. Introduction

Ensuring steady-state stability of electric power systems requires maintaining sufficient voltage stability margins. These margins provide a metric of the distance to voltage-collapse induced blackouts. Specifically, voltage stability margins measure the distance from a specified operating point to the power flow solvability boundary in a given direction of power injection variation.

There is a large literature regarding voltage stability analyses. Both saddle-node bifurcations, whereby two power flow solutions annihilate each other, and limit-induced bifurcations, whereby encountering a limit qualitatively changes component behavior, can result in voltage instability [1]–[11].

Voltage stability margins are commonly calculated using methods based on continuation and optimization. Continuation-based methods repeatedly calculate power flow solutions to find the “nose” point of a power versus

voltage (“P–V”) curve while monitoring “reactive margins” on generators (i.e., the margin between the generator’s reactive power output at a given operating point and its maximum reactive output) [4], [6], [12]. Upon reaching a reactive power limit, a generator is switched from maintaining a constant voltage magnitude to a constant reactive power output at the corresponding limit [13]. Industry standards include [9], [10], [14]. Optimization-based methods directly calculate voltage stability margins by maximizing a loading parameter subject to power flow constraints and component limits [3].

To achieve consistency between the optimization- and continuation-based methods, [15] proposes an optimization formulation with complementarity constraints to model reactive-power-limited generators. Under some generically satisfied technical conditions, [16] proves that any local solution to the optimization formulation of [15] is either a limit-induced or saddle-node bifurcation.

Many of the techniques for calculating voltage stability margins are mature and tractable for large-scale systems. However, typical existing techniques are only guaranteed to find a *local* maximum of the distance to the power flow solvability boundary; the non-convexity of the power flow feasible space implies the potential existence of multiple local maxima to the optimization problem corresponding to the voltage stability margin calculation. That is, there may be feasible regions allowing stable operation beyond the nose point identified by traditional voltage stability margin calculation techniques.<sup>1</sup> (Section 5 of this paper provides a small example system exhibiting this behavior.) Traditional local techniques are only guaranteed to find a *lower bound* on the voltage stability margin.

Existing techniques also have challenges with choosing an appropriate initialization. Continuation-based methods require an initialization that satisfies all power flow and generator capability constraints, which can be difficult to determine. The convergence and optimality characteristics of the non-convex optimization formulations [15], [16]

1. Note that the loading parameter typically cannot be locally increased beyond a local maximum in the originally specified direction, but an alternate loading path may yield a region of stable operation further in the originally specified loading direction.

*The authors acknowledge the support of the Dow Postdoctoral Fellowship in Sustainability, ARPA-E grant DE-AR0000232, and Los Alamos National Laboratory subcontract 270958.*

depend on the choice of initialization. In many operational settings, initialization from the state estimator is likely to be suitable. The importance of the initialization is more apparent for planning purposes or after a large operational change without a known operating point.

To supplement existing methods, previous work [17] has proposed a semidefinite programming (SDP) relaxation whose solution yields an upper bound on the voltage stability margin. Solution of this convex SDP relaxation does not depend on the initialization. Further, the SDP relaxation is proven to be feasible, ensuring reliable calculation of the voltage stability margin. By exploiting network sparsity [18], [19], the SDP relaxation is computationally tractable for large systems.

The SDP relaxation is *exact* if its solution satisfies a rank condition. This indicates that the upper bound provided by the SDP relaxation is tight and the nose point can be obtained directly. However, the bound on the voltage stability margin provided by the SDP relaxation is valid regardless of the solution’s rank characteristics.

The work in [17] models generators as ideal voltage sources regardless of their reactive power output. Two formulations that consider reactive-power-limited generators are proposed in [20]. The first reformulates the complementarity conditions in [15] using integer constraints to obtain a mixed-integer SDP relaxation. The second develops infeasibility certificates using sum-of-squares programming. Both formulations are computationally limited to small problems.

To achieve large-scale computational tractability, this paper proposes a further relaxation of the SDP formulation described in [17]. Specifically, this paper employs a convex second-order cone programming (SOCP) relaxation of the power flow equations adopted from [21]. This paper also presents a further relaxation for cases that only enforce upper limits on reactive power generation.

Computation of the SOCP relaxation is significantly faster than the SDP relaxation. Additionally, by applying a commercial solver (e.g., MOSEK) to the mixed-integer SOCP problems corresponding to voltage stability margins with reactive-power-limited generators, systems with thousands of buses are computationally tractable. The intermediate results from the mixed-integer SOCP solver provide useful upper bounds on the voltage stability margins within a few seconds. These computational advantages come at the cost of tightness of the SOCP bounds in comparison to the SDP bounds. This paper analyzes the trade-off between computational speed and tightness using large-scale test cases representing portions of European power systems.

Closely related to calculating voltage stability margins, there has been significant work on conditions proving the existence or non-existence of power flow solutions. We next present a selection of the broad literature on this topic. Reference [22] describes (often conservative)

sufficient conditions for power flow solution existence. Other work includes [23] and [24], which analyze approximate forms of the power flow equations. Reference [25] describes a modified Newton-Raphson iteration tailored to handle ill-conditioning. References [26] and [27] calculate the voltage profile with the closest power injections to those specified. The worst-case load shedding necessary for power flow solvability is discussed in [28].

Certifying power flow insolvability is not possible with traditional techniques, such as Newton-Raphson, which only yield locally optimal solutions and depend on the chosen initialization. Further, existing work often does not consider generators with reactive power limits; power flow equations identified as solvable under the conditions in many of these works may not have any solutions within the generators’ reactive power capabilities.

Leveraging the ability to globally solve the convex SDP relaxation, previous work [17] develops sufficient conditions for insolvability of the power flow equations, including consideration of reactive-power-limited generators [20]. By appropriate selection of the loading direction, the convex relaxations give a specific voltage stability margin as a factor of the specified power injections. If this margin is less than one, the specified set of power flow equations is infeasible. This paper extends the work in [17] and [20] to develop computationally advantageous SOCP-based insolvability conditions.

This paper is organized as follows. Section 2 overviews the power flow equations including reactive-power-limited generators. Section 3 reviews the optimization problem used to calculate voltage stability margins. Section 4 first describes the SDP relaxation developed in [17] and [20] and then presents the SOCP relaxation for the voltage stability margin calculation and power flow insolvability certification. Section 5 presents an illustrative example. Section 6 provides numerical results comparing the tightness and computational burden of the relaxations. Section 7 concludes the paper.

## 2. Overview of Power Flow Equations

The power flow equations describe the sinusoidal steady state equilibrium of a power network, and hence are formulated in terms of a complex “phasor” representation of circuit quantities. The non-linear relationship between the voltage phasors and the power injections results in non-linearity of the power flow equations.

Denote the complex voltage phasors as  $V$  and the network admittance matrix as  $\mathbf{Y}$ .<sup>2</sup> Using “active/reactive” representation of complex power injections  $P_k + jQ_k$ , where  $j = \sqrt{-1}$ , power balance at bus  $k$  yields

2. The voltage phasors are often represented by real quantities using either polar coordinates (i.e.,  $V_k = |V_k|e^{j\theta_k}$ ) or rectangular coordinates ( $V_k = V_{dk} + jV_{qk}$ ). We maintain a complex representation in order to more naturally introduce the SDP relaxation in Section 4.1.

$$\operatorname{Re}(V_k (\overline{\mathbf{Y}}_k \cdot \overline{\mathbf{V}})) = P_k \quad (1a)$$

$$\operatorname{Im}(V_k (\overline{\mathbf{Y}}_k \cdot \overline{\mathbf{V}})) = Q_k \quad (1b)$$

where  $\overline{(\cdot)}$  indicates the complex conjugate operator,  $\operatorname{Re}(\cdot)$  and  $\operatorname{Im}(\cdot)$  represent the real and imaginary parts of a complex quantity, and subscripts indicate the corresponding vector or matrix entry, with subscript  $k$  denoting the  $k^{\text{th}}$  row of a matrix.

The squared voltage magnitude at bus  $i$  is

$$V_k \overline{V}_k = |V_k|^2 \quad (1c)$$

where  $|\cdot|$  denotes the magnitude.

To represent typical equipment behavior, each bus is traditionally classified as PQ, PV, or slack. PQ buses, which typically correspond to loads and are denoted by the set  $\mathcal{PQ}$ , treat  $P_k$  and  $Q_k$  as specified quantities and enforce the active power (1a) and reactive power (1b) equations. PV buses, which typically correspond to generators and are denoted by the set  $\mathcal{PV}$ , enforce (1a) and (1c) with specified  $P_k$  and  $|V_k|^2$ . The associated reactive power  $Q_i$  may be computed as an “output quantity” via (1b). Finally, a single slack bus is selected with specified  $V_k$  (typically chosen such that the reference angle is  $0^\circ$ , i.e.,  $\operatorname{Im}(V_k) = 0$ ). The set  $\mathcal{S}$  denotes the slack bus. The active power  $P_k$  and reactive power  $Q_k$  at the slack bus are determined from (1a) and (1b); network-wide conservation of complex power is thereby satisfied.

Note that while we consider a constant-power load model, more general “ZIP” models which also have constant-current and constant-impedance components can be incorporated into the convex relaxations [29].

Additionally, generator reactive power outputs must be within specified limits. If a generator’s reactive power output is between the upper and lower limits, the generator maintains a constant voltage magnitude at the bus (i.e., behaves like a PV bus). If a generator’s reactive power output reaches its upper limit, the reactive power output is fixed at the upper limit and the bus voltage magnitude is allowed to decrease (i.e., behaves like a PQ bus with reactive power injection given by the upper limit). If the generator’s reactive power output reaches its lower limit, the reactive power output is fixed at the lower limit and the voltage magnitude is allowed to increase (i.e., the bus behaves like a PQ bus with reactive power injection determined by the lower limit). Figure 1 shows this reactive power versus voltage characteristic with a voltage magnitude setpoint of  $V^*$  and lower and upper reactive power limits of  $Q^{\min}$  and  $Q^{\max}$ .

### 3. Non-Convex Optimization Formulation for Calculating Voltage Stability Margins

This section reviews a non-convex optimization problem adopted from [15] whose solution provides a voltage

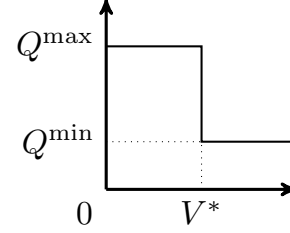


Figure 1. Reactive Power vs. Voltage Characteristic

stability margin. This problem maximizes a parameter  $\eta$  in a specified loading direction (typically a direction of changing power injections, i.e., the right hand sides of (1a) and (1b)). The optimization problem is constrained by the power flow equations with one degree of freedom in the specified loading direction:

$$\max_{V, \eta, \psi_L, \psi_U} \eta \quad \text{subject to} \quad (2a)$$

$$\operatorname{Re}(V_k (\overline{\mathbf{Y}}_k \cdot \overline{\mathbf{V}})) = P_k(\eta) \quad \forall k \in \{\mathcal{PQ}, \mathcal{PV}\} \quad (2b)$$

$$\operatorname{Im}(V_k (\overline{\mathbf{Y}}_k \cdot \overline{\mathbf{V}})) = Q_k(\eta) \quad \forall k \in \mathcal{PQ} \quad (2c)$$

$$\begin{cases} \operatorname{Im}(V_k (\overline{\mathbf{Y}}_k \cdot \overline{\mathbf{V}})) \geq Q_k^{\max} \psi_{Uk} + Q_k^{\min} (1 - \psi_{Uk}) \\ \operatorname{Im}(V_k (\overline{\mathbf{Y}}_k \cdot \overline{\mathbf{V}})) \leq Q_k^{\min} \psi_{Lk} + Q_k^{\max} (1 - \psi_{Lk}) \end{cases} \quad \forall k \in \{\mathcal{PV}, \mathcal{S}\} \quad (2d)$$

$$\begin{cases} V_k \overline{V}_k \geq |V_k^*|^2 (1 - \psi_{Uk}) \\ V_k \overline{V}_k \leq |V_k^*|^2 (1 - \psi_{Lk}) + M \psi_{Lk} \end{cases} \quad \forall k \in \{\mathcal{PV}, \mathcal{S}\} \quad (2e)$$

$$\psi_{Lk} + \psi_{Uk} \leq 1 \quad \forall k \in \{\mathcal{PV}, \mathcal{S}\} \quad (2f)$$

$$\sum_{k \in \{\mathcal{PV}, \mathcal{S}\}} (\psi_{Lk} + \psi_{Uk}) \leq n_g - 1 \quad (2g)$$

$$\psi_{Uk} \in \{0, 1\} \quad \psi_{Lk} \in \{0, 1\} \quad \forall k \in \{\mathcal{PV}, \mathcal{S}\} \quad (2h)$$

where  $n_g$  is the number of PV and slack buses;  $M$  is a large constant;  $P_k(\eta)$  and  $Q_k(\eta)$  are specified linear functions of  $\eta$  providing the active and reactive power loading directions, respectively, at bus  $k$ ; and  $V_k^*$  denotes specified voltage magnitudes at slack and PV buses.

Equations (2b) and (2c) correspond to the power flow equations (1a) and (1b). Equations (2d)–(2h) use binary variables to implement the complementarity constraints from [15] that model the reactive power versus voltage magnitude characteristic shown in Figure 1. When the binary variable  $\psi_{Uk}$  is equal to one, the upper reactive power limit of the generator at bus  $k$  is binding. Accordingly, (2d) fixes the reactive power output at the upper limit and (2e) sets the lower voltage magnitude limit to zero. When the binary variable  $\psi_{Lk}$  is equal to one, the lower reactive power limit of the generator at bus  $k$  is binding. Accordingly, (2d) fixes the generator reactive power output at the lower limit and (2e) removes the upper voltage magnitude limit. When both  $\psi_{Uk} = 0$  and  $\psi_{Lk} = 0$ , (2d) constrains the reactive power output within the upper and lower limits and (2e) fixes the voltage

magnitude to the specified value  $V_k^*$ . Consistency in the reactive power limits is enforced by (2f); a generator's reactive power output cannot simultaneously be at both the upper and lower limits. Constraint (2g) ensures the existence of at least one voltage-controlled bus. This is not necessary but improves convergence characteristics. The optimal solution to (2), denoted  $\eta^*$ , provides a stability margin in the specified loading direction.

## 4. Convex Relaxations

This section employs convex SDP and SOCP relaxations of the non-convex power flow equations (1) to upper bound the voltage stability margin  $\eta^*$  from (2). The formulations in this section are developed from relaxations of optimal power flow problems in [30] and [21]. When combined with the integer constraints in (2d)–(2h), the resulting formulations are mixed-integer SDP and mixed-integer SOCP problems. Despite the non-convexity resulting from the integer constraints, global solution of these problems is enabled by the convexity of the underlying relaxations of the power flow equations and the availability of lower and upper bounding techniques for mixed-integer conic programs [31], [32].<sup>3</sup> The SDP relaxation was first presented in [17] and extended to handle reactive-power-limited generators in [20]. The SOCP relaxation is the main contribution of this paper.

### 4.1. SDP Relaxation

Using the quadratic relationship between the power injections and the voltage phasors, the SDP relaxation is developed by isolating the power flow non-convexity to a rank constraint. Relaxation of this rank constraint to a less stringent positive semidefinite matrix constraint yields the SDP relaxation.

Denote the  $k^{\text{th}}$  column of the  $n \times n$  identity matrix as  $e_k$ . Define the Hermitian matrices

$$\mathbf{H}_k = \frac{\mathbf{Y}^H e_k e_k^T + e_k e_k^T \mathbf{Y}}{2} \quad (3)$$

$$\tilde{\mathbf{H}}_k = \frac{\mathbf{Y}^H e_k e_k^T - e_k e_k^T \mathbf{Y}}{2\mathbf{j}} \quad (4)$$

where  $(\cdot)^T$  and  $(\cdot)^H$  indicate the transpose and conjugate transpose, respectively. Let  $\mathbf{W}$  denote the  $n \times n$  rank-one Hermitian matrix

$$\mathbf{W} = VV^H \quad (5)$$

The active and reactive power injections are

3. When the meaning is clear from the context, we occasionally abuse terminology by referring to formulations with both convex constraints and non-convex integer variables as “convex relaxations.”

$$P_k = \text{tr}(\mathbf{H}_k \mathbf{W}) \quad (6a)$$

$$Q_k = \text{tr}(\tilde{\mathbf{H}}_k \mathbf{W}) \quad (6b)$$

where  $\text{tr}(\cdot)$  is the trace operator. The squared voltage magnitudes are

$$|V_k|^2 = \text{tr}(e_k e_k^T \mathbf{W}) \quad (6c)$$

The expressions in (6) are linear in the entries of  $\mathbf{W}$ . Thus, all the non-linearity is isolated to the rank constraint (5). The SDP relaxation is formed by using (6) to replace all terms involving  $V$  in (2) with terms involving  $\mathbf{W}$  and then relaxing the rank constraint  $\mathbf{W} = VV^H$  to the positive semidefinite matrix constraint  $\mathbf{W} \succeq 0$ :

$$\max_{\mathbf{w}, \eta, \psi_L, \psi_U} \eta \quad \text{subject to} \quad (7a)$$

$$\text{tr}(\mathbf{H}_k \mathbf{W}) = P_k(\eta) \quad \forall k \in \{\mathcal{PQ}, \mathcal{PV}\} \quad (7b)$$

$$\text{tr}(\tilde{\mathbf{H}}_k \mathbf{W}) = Q_k(\eta) \quad \forall k \in \mathcal{PQ} \quad (7c)$$

$$\begin{cases} \text{tr}(\tilde{\mathbf{H}}_k \mathbf{W}) \geq Q_k^{\max} \psi_{Uk} + Q_k^{\min} (1 - \psi_{Uk}) \\ \text{tr}(\tilde{\mathbf{H}}_k \mathbf{W}) \leq Q_k^{\min} \psi_{Lk} + Q_k^{\max} (1 - \psi_{Lk}) \end{cases} \quad \forall k \in \{\mathcal{PV}, \mathcal{S}\} \quad (7d)$$

$$\begin{cases} \text{tr}(e_k e_k^T \mathbf{W}) \geq (V_k^*)^2 (1 - \psi_{Uk}) \\ \text{tr}(e_k e_k^T \mathbf{W}) \leq (V_k^*)^2 (1 - \psi_{Lk}) + M \psi_{Lk} \end{cases} \quad \forall k \in \{\mathcal{PV}, \mathcal{S}\} \quad (7e)$$

$$\mathbf{W} \succeq 0 \quad (7f)$$

$$\psi_{Lk} + \psi_{Uk} \leq 1 \quad \forall k \in \{\mathcal{PV}, \mathcal{S}\} \quad (7g)$$

$$\sum_{k \in \{\mathcal{PV}, \mathcal{S}\}} (\psi_{Lk} + \psi_{Uk}) \leq n_g - 1 \quad (7h)$$

$$\psi_{Uk} \in \{0, 1\} \quad \psi_{Lk} \in \{0, 1\} \quad \forall k \in \{\mathcal{PV}, \mathcal{S}\} \quad (7i)$$

Denote the globally optimal objective value to (7) as  $\eta_{SDP}^*$ .

A global solution to the SDP relaxation which satisfies the rank condition (5) is *exact* and thus yields both the globally maximal voltage stability margin and the voltage phasors at the “nose point” of the P–V curve. However,  $\eta_{SDP}^*$  provides an upper bound on the voltage stability margin even if the rank condition (5) is not satisfied.

Without consideration of reactive power limits (i.e.,  $Q_k^{\max} = -Q_k^{\min} = \infty$ ,  $\psi_{Uk} = \psi_{Lk} = 0$ ,  $\forall k \in \{\mathcal{PV}, \mathcal{S}\}$ ), the SDP relaxation is equivalent to the formulation in [17]. By exploiting network sparsity, calculation of voltage stability margins for large systems is computationally tractable [18], [19].

The formulation with consideration of reactive power limits, first presented in [20], is a mixed-integer SDP. Mixed-integer SDP solvers, such as YALMIP's branch-and-bound algorithm [31], are not mature and the applicability of (7) is thus limited to small systems.

## 4.2. SOCP Relaxation

Computational difficulties related to the immaturity of mixed-integer SDP solvers motivates the development of more computationally tractable alternatives to the formulation in Section 4.1. This section presents a computationally advantageous mixed-integer SOCP relaxation.

We use the ‘‘branch-flow model’’ (BFM) relaxation of the power flow equations from [21]. The BFM has the same optimal objective value as a relaxation of the complex SDP constraint  $\mathbf{W} \succeq 0$  to less stringent SOCP constraints (i.e., the ‘‘bus-injection model’’ relaxation in [21]). The BFM is selected due to its superior numeric characteristics [33].

The BFM relaxes the DistFlow equations [34], which formulate the power flow equations in terms of active power, reactive power, and squared current magnitude flows,  $P_{lm}$ ,  $Q_{lm}$ , and  $L_{lm}$ , respectively, into terminal  $l$  of the line connecting buses  $l$  and  $m$  as well as squared voltage magnitudes  $|V_k|^2$  at each bus  $k$ .

As shown in Figure 2, consider a line model with an ideal transformer that has a specified turns ratio  $\tau_{lm}e^{j\theta_{lm}} : 1$  in series with a  $\Pi$  circuit with series impedance  $R_{lm} + \mathbf{j}X_{lm}$  and shunt admittance  $\mathbf{j}b_{sh,lm}$ .

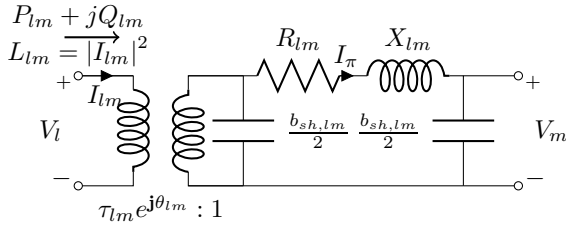


Figure 2. Line Model

To derive the BFM relaxation, we begin with the relationship between the active and reactive line flows and the squared current magnitude:

$$L_{lm} \cdot |V_l|^2 = P_{lm}^2 + Q_{lm}^2 \quad (8)$$

To form a SOCP, (8) is relaxed to an inequality constraint:

$$L_{lm} \cdot |V_l|^2 \geq P_{lm}^2 + Q_{lm}^2 \quad (9)$$

The current flow on the series impedance of the  $\Pi$ -circuit model is

$$I_{\pi} = \left( \frac{P_{lm} - \mathbf{j}Q_{lm}}{\bar{V}_l} \right) (\tau_{lm}e^{-j\theta_{lm}}) - \mathbf{j} \frac{b_{sh,lm}V_l}{2\tau_{lm}e^{j\theta_{lm}}} \quad (10)$$

The relationship between the terminal voltages is

$$\frac{V_l}{\tau_{lm}e^{j\theta_{lm}}} - I_{\pi} (R_{lm} + \mathbf{j}X_{lm}) = V_m \quad (11)$$

Taking the squared magnitude of both sides of (11) and using (8) and (10) yields

$$\begin{aligned} |V_m|^2 &= \frac{|V_l|^2}{\tau_{lm}^2} - 2(X_{lm}Q_{lm} + R_{lm}P_{lm}) - |V_l|^2 X_{lm} \frac{b_{sh,lm}}{\tau_{lm}^2} \\ &\quad + (R_{lm}^2 + X_{lm}^2) \left( Q_{lm}b_{sh,lm} + \tau_{lm}^2 L_{lm} + \frac{b_{sh,lm}^2 |V_l|^2}{4\tau_{lm}^2} \right) \end{aligned} \quad (12)$$

Active and reactive line losses are

$$P_{loss,lm} = R_{lm}\tau_{lm}^2 L_{lm} + \frac{R_{lm}b_{sh,lm}^2}{4\tau_{lm}^2} |V_l|^2 + Q_{lm}R_{lm}b_{sh,lm} \quad (13a)$$

$$Q_{loss,lm} = X_{lm}\tau_{lm}^2 L_{lm} + \left( \frac{X_{lm}b_{sh,lm}^2 - 2b_{sh,lm}}{4\tau_{lm}^2} \right) |V_l|^2 \quad (13b)$$

The active and reactive injections at bus  $k$  are

$$P_k^{SOCP} = \sum_{\substack{\{(l,m) \in \mathcal{L} \\ \text{s.t. } l=k\}}} P_{lm} + \sum_{\substack{\{(l,m) \in \mathcal{L} \\ \text{s.t. } m=k\}}} (P_{loss,lm} - P_{lm}) + g_{sh,k} |V_k|^2 \quad (14a)$$

$$Q_k^{SOCP} = \sum_{\substack{\{(l,m) \in \mathcal{L} \\ \text{s.t. } l=k\}}} Q_{lm} + \sum_{\substack{\{(l,m) \in \mathcal{L} \\ \text{s.t. } m=k\}}} (Q_{loss,lm} - Q_{lm}) + b_{sh,k} |V_k|^2 \quad (14b)$$

where  $g_{sh,k} + \mathbf{j}b_{sh,k}$  is the shunt admittance at bus  $k$  and  $\mathcal{L}$  represents the set of all lines.

The BFM-based SOCP relaxation of (2) is

$$\max_{P_{lm}, Q_{lm}, L_{lm}, |V_k|^2, \eta, \psi_{Lk}, \psi_{Uk}} \eta \quad \text{subject to} \quad (15a)$$

$$P_k^{SOCP} = P_k(\eta) \quad \forall k \in \{\mathcal{PQ}, \mathcal{PV}\} \quad (15b)$$

$$Q_k^{SOCP} = Q_k(\eta) \quad \forall k \in \mathcal{PQ} \quad (15c)$$

$$\begin{cases} Q_k^{SOCP} \geq Q_k^{max} \psi_{Uk} + Q_k^{min} (1 - \psi_{Uk}) \\ Q_k^{SOCP} \leq Q_k^{min} \psi_{Lk} + Q_k^{max} (1 - \psi_{Lk}) \end{cases} \quad \forall k \in \{\mathcal{PV}, \mathcal{S}\} \quad (15d)$$

$$\begin{cases} |V_k|^2 \geq (V_k^*)^2 (1 - \psi_{Uk}) \\ |V_k|^2 \leq (V_k^*)^2 (1 - \psi_{Lk}) + M\psi_{Lk} \end{cases} \quad \forall k \in \{\mathcal{PV}, \mathcal{S}\} \quad (15e)$$

$$\psi_{Lk} + \psi_{Uk} \leq 1 \quad \forall k \in \{\mathcal{PV}, \mathcal{S}\} \quad (15f)$$

$$\sum_{k \in \{\mathcal{PV}, \mathcal{S}\}} (\psi_{Lk} + \psi_{Uk}) \leq n_g - 1 \quad (15g)$$

$$\psi_{Uk} \in \{0, 1\} \quad \psi_{Lk} \in \{0, 1\} \quad \forall k \in \{\mathcal{PV}, \mathcal{S}\} \quad (15h)$$

Eqns. (9) and (12)–(14)

Denote the globally optimal objective value to (15) as  $\eta_{SOCP}^*$ .

Without consideration of reactive power limits (i.e.,  $Q_k^{max} = -Q_k^{min} = \infty$ ,  $\psi_{Uk} = \psi_{Lk} = 0$ ,  $\forall k \in \{\mathcal{PV}, \mathcal{S}\}$ ), (15) is a SOCP that can be solved efficiently with commercial solvers.

With consideration of reactive power limits, (15) is a mixed-integer SOCP. Solvers for mixed-integer SOCP

problems, such as MOSEK, are significantly more mature than mixed-integer SDP solvers. The SOCP relaxation (15) is therefore applicable to large systems with thousands of buses. At each iteration, a typical mixed-integer SOCP solver calculates an upper bound on the optimal objective value by relaxing the integer constraints using techniques such as those described in [32]. Thus, each iteration provides an upper bound on the voltage stability margin, and waiting for full convergence of (15) is not required. As shown in the results in Section 6, quality bounds on the voltage stability margin are often available within a few seconds even for large systems.

The computational speed advantage of the SOCP relaxation comes at the cost of the relaxation's tightness, with the SDP relaxation generally yielding superior upper bounds. Section 6 explores the trade-off between tightness and computational speed for a variety of large test cases.

### 4.3. Enforcing Only Upper Reactive Limits

Under the high loading conditions associated with voltage stability, the upper reactive power limits are significantly more relevant operational constraints than lower limits. Neglecting lower reactive power limits enables the development of convex relaxations that do not require integer constraints. As will be shown in Section 6, these relaxations are often superior to enforcing the integer constraints when lower reactive power limits are neglected.

In the absence of lower reactive power limits (i.e.,  $Q^{min} = -\infty$ ), the generator capability curve shown in Figure 1 is the border of the convex region defined by  $0 \leq V \leq V^*$  and  $Q \leq Q^{max}$ . Thus, a relaxation of the reactive power capability curve is formed by replacing (2d)–(2h) with

$$V_k \bar{V}_k \leq |V_k^*|^2 \quad (16a)$$

$$\text{Im}(V_k (\bar{\mathbf{Y}}_k \cdot \bar{\mathbf{V}})) \leq Q_k^{max} \quad (16b)$$

Accordingly modifying the SDP and SOCP relaxations yields formulations without integer constraints.

### 4.4. Certifying Power Flow Insolvability

The ability to globally solve the relaxations in this section enables the development of sufficient conditions for power flow insolvability, which is not possible with conventional Newton-based algorithms.

Consider a loading direction with uniformly changing power injections at constant power factor:  $P_k(\eta) = P_{k0} \eta$  and  $Q_k(\eta) = Q_{k0} \eta$ , where  $P_{k0}$  and  $Q_{k0}$  are the specified power injections for the power flow equations.

Since  $\eta_{SDP}^*$  and  $\eta_{SOCP}^*$  upper bound a measure of the distance to the power flow solvability boundary,

$$\eta_{SDP}^* < 1 \quad (17a)$$

$$\eta_{SOCP}^* < 1 \quad (17b)$$

are sufficient conditions for power flow insolvability. We emphasize that these are *sufficient* but not *necessary* conditions: failure to satisfy (17) does not certify that a power flow solution exists due to the potential *relaxation gap* between the solution to a convex relaxation and the global solution to (2). To potentially speed computation, an upper bound obtained at any solver iteration can be used to evaluate (17). Further, if lower reactive power limits are neglected, these conditions are also valid for bounds produced using the relaxation in Section 4.3.

Without consideration of reactive power limits, [17] proves that (2) is feasible, and thus the insolvability conditions can always be evaluated. On the other hand, there is no feasibility proof for (2) when reactive power limits are enforced. It may therefore be possible to specify a power flow problem with reactive power limits for which the insolvability conditions cannot be evaluated.

## 5. Illustrative Example

The optimization problem (2) is a mixed-integer nonlinear program, a class of problems which are generally difficult to solve. Further, (2) inherits the non-convexity of the power flow equations. It may therefore have local optima even in the absence of reactive power limits. We next present a small test case adopted from [35] which illustrates the potential non-convexity of (2). Figure 3 shows the one-line diagram for this test case. The generators maintain voltage magnitudes of 1 per unit at each bus without reactive power limits.

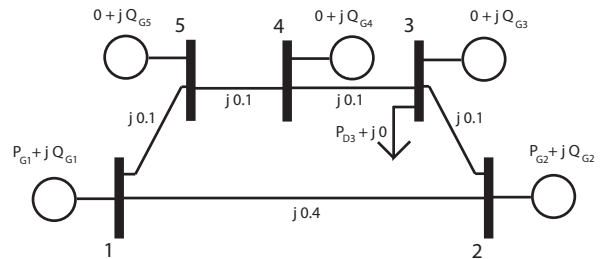


Figure 3. Diagram for Five-Bus System in [35]

The non-convex feasible space for this test case, projected onto the set of active power injections at buses 1 and 2, is shown by the light gray region in Figure 4. Consider a direction of power injection increase of  $[P_{G2} \ P_{G3} \ P_{G4} \ P_{G5}]^T = [12.27 \ -(12.27 + \eta) \ 0 \ 0]^T$  per unit, where  $\eta$  is the degree of freedom (increasing  $\eta$  corresponds to increasing the active power demand at bus 3). Since the system is lossless, the power supplied by the slack bus

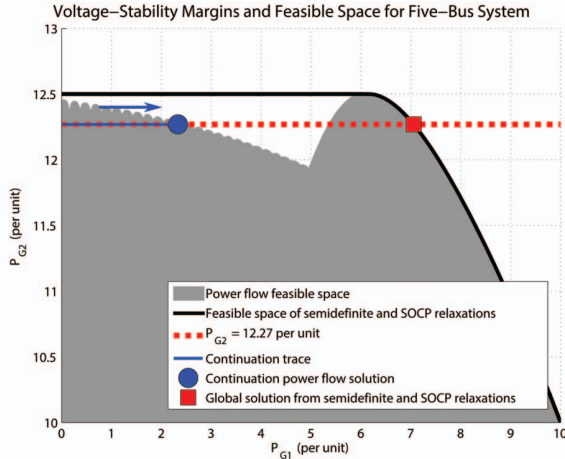


Figure 4. Feasible Space for Five-Bus System in [35]

$P_{G1} = \eta$  per unit. This direction is indicated by the red dashed line in Figure 4. A local solution method (e.g., continuation) initialized at a point on the red line with  $0 \leq \eta = P_{G1} \leq 2.33$  per unit finds the local maximum at  $\eta = 2.33$  per unit, denoted by the blue dot on Figure 4.

Choosing an initial condition corresponding to  $5.41 \leq \eta \leq 7.05$  per unit or a different loading trajectory (i.e., a path that goes around the non-convexity in Figure 4) would identify solutions further in the originally specified loading direction. Thus, this example illustrates that local solution techniques are dependent on the initialization and may have local maxima.

Conversely, the feasible space of power injections for both the SDP and SOCP relaxations is the interior of the solid black curve. For the specified direction, solving either relaxation directly yields the global maximum  $\eta = 7.05$  per unit, which is located at the red square in Figure 4, without the need to specify an initialization.

This example illustrates some of the advantages and disadvantages of both the traditional and convex relaxation approaches. For this problem, the convex relaxations identify (and, more generally, upper bound) the global maximum of the voltage stability margin. Thus, the relaxations guarantee that no power flow solution exists in the specified direction beyond  $\eta = 7.05$  per unit. Conversely, identification of the local maximum (i.e., the nose point) from a continuation method does not preclude the existence of power flow solutions for larger loadings.

On the other hand, the convex relaxations do not find the bifurcation that occurs along the originally specified loading direction which is identified by the continuation method. In other words, the relaxations do not indicate the infeasible region that exists for  $2.33 < \eta < 5.41$  per unit. The start of this infeasible region is identified by a continuation method.

Thus, the traditional methods and the convex relax-

ations work well in concert by proving lower and upper bounds, respectively. A large gap between these bounds suggests a problem worthy of further investigation (e.g., testing alternative loading paths).

## 6. Results

This section presents results from applying the relaxations to both small problems and large test cases representing portions of European power systems. Test cases both with and without enforcement of reactive power limits are considered. We use the IEEE test cases [36] and large test cases representing the Great Britain (GB) [37] and Poland (PL) [38] power systems as well as other European power systems from the PEGASE project [39]. These large test cases were pre-processed to remove low-impedance lines as described in [40] in order to improve the solver's numerical convergence. A  $1 \times 10^{-3}$  per unit low-impedance line threshold was used for all test cases except for PEGASE-1354, PEGASE-2869, and PEGASE-9241 which use a  $3 \times 10^{-3}$  per unit threshold.

The power injection direction is specified with uniformly changing active and reactive power injections at constant power factor:  $P_k(\eta) = P_{k0}\eta$  and  $Q_k(\eta) = Q_{k0}\eta$ , where  $P_{k0}$  and  $Q_{k0}$  are the test cases' specified power injections. The condition from Section 4.4 thus guarantees that increasing power injections by more than the value of  $\eta$  implied by these results will yield an insolvable set of power flow equations.

The relaxations are implemented using MATLAB 2013a, YALMIP 2014.06.05 [31], and Mosek 7.1.0.28. The relaxations were solved using a computer with a quad-core 2.70 GHz processor and 16 GB of RAM. The "solver time" results do not include the typically small problem formulation times.

The continuation power flow (CPF) in MATPOWER [38], modified to consider reactive-power-limited generators, is used to obtain a lower bound on the voltage stability margin. In order to maintain consistency between the CPF and convex relaxations, we do not limit the slack bus reactive power output.<sup>4</sup> Solution times for the CPF method are not provided for the results in this section due to a strong dependence on implementation details (e.g., selected step sizes, tolerances, and methods for identifying reactive power limit violations). We note that commercial continuation codes are tractable for large systems.

The upper bounds provided by the convex relaxations are reported as a *relaxation gap* calculated as the percent difference from the nose point identified by the CPF. Thus, the relaxation gap is determined by both the CPF's

4. When the slack bus encounters a reactive power limit, this particular CPF switches the slack bus to a PQ bus and chooses a new PV bus to serve as the slack bus. This has the potential to make the active power differ from the specified power injection direction.

lower bound and the relaxation's upper bound. Future work includes determining the relative contribution of each bound to the relaxation gap (i.e., whether a feasible region exists between the nose point identified by the CPF and the upper bound from the relaxations).

### 6.1. Without Reactive Power Limits

Table 1 presents results for the test cases without enforcing reactive power limits (i.e.,  $Q_k^{max} = -Q_k^{min} = \infty$ ,  $\psi_{Uk} = \psi_{Lk} = 0$ ,  $\forall k \in \{\mathcal{PV}, \mathcal{S}\}$ ).

Table 1. Voltage Stability Margins Without Enforcing Reactive Power Limits

Case Name	SDP		SOCP	
	Gap (%)	Time (sec)	Gap (%)	Time (sec)
IEEE-9	0.00	0.5	1.30	0.6
IEEE-14	0.00	0.5	6.30	0.5
IEEE-30	0.00	0.5	0.27	0.5
IEEE-39	0.00	0.5	0.37	0.5
IEEE-57	0.00	0.5	1.88	0.5
IEEE-118	2.63	0.9	5.83	0.6
IEEE-300	0.00	0.9	0.03	0.6
GB-2224	0.90	3.2	2.48	1.2
PL-2383wp	2.20	7.4	4.96	0.8
PL-2736sp	0.37	9.0	3.13	0.9
PL-2737sop	3.76	6.6	13.03	0.9
PL-2746wop	3.55	10.0	11.33	0.8
PL-2746wp	1.31	5.9	2.20	0.3
PL-3012wp	2.33	7.4	10.78	1.0
PL-3120sp	2.00	7.6	11.82	1.0
PEGASE-89	0.10	0.6	0.46	0.5
PEGASE-1354	0.42	2.0	0.64	0.7
PEGASE-2869	1.16	5.3	3.36	1.0
PEGASE-9241	0.33	42.7	0.13	2.8

Table 1 illustrates a trade-off between computational speed and tightness of the convex relaxations. For the larger systems, the SOCP relaxation is between a factor of 2.6 and 16.8 faster than the SDP relaxation. However, the SOCP relaxation has relaxation gaps that are up to 9.26% larger than the SDP relaxation.<sup>5</sup> The SDP relaxation is exact (i.e., finds the nose point) for all IEEE systems except IEEE-118, and the worst relaxation gap among all the test cases is 3.76%. With relaxation gaps between 0.03% and 13.03%, the SOCP relaxation also yields useful upper bounds on the voltage stability margins.

### 6.2. With Reactive Power Limits

Table 2 presents results for the small IEEE test cases with enforcement of both upper and lower reactive power limits. The SDP and SOCP relaxations are both computationally tractable for these test cases, although the SOCP relaxation is significantly faster for IEEE-39 and IEEE-57. The SDP relaxation is exact for all of these test cases, and the SOCP relaxation has small relaxation gaps.

5. The SDP relaxation gap for PEGASE-9241 is slightly greater than the SOCP gap due to numerical issues with the SDP solution.

Table 2. Voltage Stability Margins Enforcing Upper and Lower Reactive Power Limits (SDP & SOCP)

Case Name	SDP		SOCP	
	Gap (%)	Time (sec)	Gap (%)	Time (sec)
IEEE-9	0.00	0.2	0.83	0.1
IEEE-14	0.00	0.1	0.21	0.1
IEEE-30	0.00	1.0	0.31	0.1
IEEE-39	0.00	65.6	0.04	0.4
IEEE-57	0.00	3.2	0.61	0.1

In contrast to the SOCP relaxation, the SDP relaxation is not computationally tractable for larger systems. Table 3 shows the upper bound from the SOCP solver after at most approximately 1000 seconds and after the first solver iteration. The SOCP relaxation yields larger gaps for the systems in Table 3 than for the smaller systems in Table 2 (up to 33.6% vs. 0.83%, respectively).

Note that the first iteration of the mixed-integer SOCP solver yields upper bounds that are often close to the bounds produced after approximately 1000 seconds of solver time. For these test cases, the first iteration yields relaxation gaps within 11.9% of the gap after 1000 seconds, and is within 2% for 8 of the 13 test cases.

Hot starting the integer variables yields significant computational improvements for some systems. For instance, hot starting with the CPF solution reduces the solver time for IEEE-300 from 316 to 108 seconds.

Table 3. Voltage Stability Margins Enforcing Upper and Lower Reactive Power Limits (SOCP)

Case Name <sup>6</sup>	SOCP (max. ~1000 sec)		SOCP (First Iter.)	
	Gap (%)	Time (sec)	Gap (%)	Time (sec)
IEEE-118	2.31	55.1	12.05	0.2
IEEE-300	1.16	315.9	13.06	0.2
GB-2224	6.47	1006.3	7.20	1.1
PL-2736sp	4.81	1009.2	8.33	0.9
PL-2737sop	6.06	1006.9	10.66	0.7
PL-2746wop	11.04	1017.9	12.74	1.0
PL-2746wp	5.96	1014.0	7.06	1.0
PL-3012wp	27.18	1006.1	28.34	1.0
PL-3120sp	33.60	1018.6	34.16	1.1
PEGASE-89	0.65	0.9	0.65	0.2
PEGASE-1354	11.51	1009.4	15.27	0.6
PEGASE-2869	10.26	1026.9	11.91	1.9
PEGASE-9241	24.71	1085.9	24.73	8.4

For practical systems and typical loading profiles, only upper bounds on reactive power injections tend to be relevant. The results in Table 4 only consider upper reactive power limits. Reinforcing the typical importance of upper limits over lower limits, the CPF nose points match to within 0.64% between consideration of both limits and only considering upper limits. The results show the first iteration of the mixed-integer SOCP relaxation<sup>7</sup>

6. Results for PL-2383wp are excluded because MATPOWER does not find a base case solution to initialize the CPF.

7. The mixed-integer SOCP relaxation converges to within 0.25% of the bound obtained from the first solver iteration for these test cases.

Table 4. Voltage Stability Margins Enforcing Only Upper Reactive Power Limits

Case Name <sup>6</sup>	SOCP (First Iter.)		$Q^{max}$ SOCP		$Q^{max}$ SDP	
	Gap (%)	Time (sec)	Gap (%)	Time (sec)	Gap (%)	Time (sec)
IEEE-118	2.37	0.2	2.37	0.5	0.00	0.9
IEEE-300	1.17	0.2	1.17	0.7	0.21	1.8
GB-2224	0.81	1.0	0.96	1.1	0.73	7.4
PL-2736sp	2.46	0.8	2.39	1.2	0.08	13.9
PL-2737sop	2.34	0.9	2.32	1.0	0.25	12.4
PL-2746wop	3.31	0.9	3.27	1.0	0.10	18.2
PL-2746wp	1.29	1.0	1.44	0.9	0.03	19.2
PL-3012wp	14.03	0.9	14.03	1.3	7.19	19.7
PL-3120sp	19.76	1.4	19.59	1.4	13.91	18.7
PEGASE-89	0.65	0.2	0.65	0.6	0.00	0.9
PEGASE-1354	0.75	0.5	0.84	0.8	0.09	4.8
PEGASE-2869	2.72	1.6	2.71	1.2	2.65	10.2
PEGASE-9241	0.59	7.8	0.62	4.2	0.31	79.6

from Section 4.2 (without lower limits) as well as the SDP and SOCP relaxations without integer constraints (columns  $Q^{max}$  SDP and  $Q^{max}$  SOCP) from Section 4.3.

The results in Table 4 show that gaps from the SOCP relaxation described in Section 4.3 are very close to those from the first iteration of the mixed-integer SOCP solver. Further, the SDP relaxation generally obtains significantly smaller gaps than the SOCP relaxations.

With relaxation gaps that are often significantly smaller than in Table 3, the results in Table 4 demonstrate that the relaxations perform better when neglecting lower reactive power limits. Neglecting lower limits imparts the physical intuition that these limits are usually significantly less relevant than upper limits. For instance, when enforcing both upper and lower limits, PL-2746wop has a relaxation gap of 11.04%. By allowing a significantly longer solver time ( $2.0 \times 10^5$  seconds on a faster workstation computer with eight cores), this case converges to obtain a relaxation gap of 3.85%. This gap is close to the 3.27% gap obtained in 1 second with the SOCP relaxation when lower reactive power limits are neglected.

To summarize the results, in the absence of reactive power limits, the SDP relaxation yields the smallest relaxation gap and the SOCP relaxation has the fastest computational speed. When considering reactive-power-limited generators, the relaxations perform best when lower reactive power limits are not enforced. In this case, the SDP and SOCP relaxations from Section 4.3 provide the smallest relaxation gap and fastest computational speed, respectively. When both upper and lower limits are enforced, the mixed-integer SDP relaxation gives the best results for small systems, but is computationally intractable for large systems. The mixed-integer SOCP relaxation gives gaps that are larger but often still useful for cases with both upper and lower reactive power limits.

## 7. Conclusion

This paper has proposed new relaxations formulated as SOCP problems for calculating voltage stability margins and certifying power flow infeasibility. When augmented with integer constraints, these relaxations consider reactive-power-limited generators. In contrast to a previous mixed-integer SDP formulation, the mixed-integer SOCP relaxations are computationally tractable for large problems. The capabilities of these relaxations are demonstrated on several large test cases representing portions of European power systems.

## References

- [1] Y. Tamura, H. Mori, and S. Iwamoto, "Relationship Between Voltage Instability and Multiple Load Flow Solutions in Electric Power Systems," *IEEE Trans. Power App. Syst.*, vol. PAS-102, no. 5, pp. 1115–1125, May 1983.
- [2] H.-D. Chiang, I. Dobson, R. Thomas, J. Thorp, and L. Fekih-Ahmed, "On Voltage Collapse in Electric Power Systems," *IEEE Trans. Power Syst.*, vol. 5, no. 2, pp. 601–611, May 1990.
- [3] T. Van Cutsem, "A Method to Compute Reactive Power Margins with Respect to Voltage Collapse," *IEEE Trans. Power Syst.*, vol. 6, no. 1, pp. 145–156, Feb. 1991.
- [4] V. Ajjarapu and C. Christy, "The Continuation Power Flow: A Tool for Steady State Voltage Stability Analysis," *IEEE Trans. Power Syst.*, vol. 7, no. 1, pp. 416–423, Feb. 1992.
- [5] I. Dobson and L. Lu, "Voltage Collapse Precipitated by the Immediate Change in Stability When Generator Reactive Power Limits are Encountered," *IEEE Trans. Circuits Syst. I, Fundam. Theory Appl.*, vol. 39, no. 9, pp. 762–766, Sept. 1992.
- [6] C. Canizares and F. Alvarado, "Point of Collapse and Continuation Methods for Large AC/DC Systems," *IEEE Trans. Power Syst.*, vol. 8, no. 1, pp. 1–8, Feb. 1993.
- [7] I. Dobson and L. Lu, "New Methods for Computing a Closest Saddle Node Bifurcation and Worst Case Load Power Margin for Voltage Collapse," *IEEE Trans. Power Syst.*, vol. 8, no. 3, pp. 905–913, Aug. 1993.
- [8] F. Alvarado, I. Dobson, and Y. Hu, "Computation of Closest Bifurcations in Power Systems," *IEEE Trans. Power Syst.*, vol. 9, no. 2, pp. 918–928, May 1994.
- [9] C. Taylor, *Power System Voltage Stability*. Electric Power Research Institute Series, McGraw-Hill, 1994.
- [10] T. Van Cutsem and C. Vournas, *Voltage Stability of Electric Power Systems*. Springer-Verlag, New York, 2008.
- [11] S.-H. Li and H.-D. Chiang, "Impact of Generator Reactive Reserve on Structure-Induced Bifurcation," in *IEEE Power Eng. Soc. General Meeting*, Jul. 2009.

- [12] G. Price, "A Generalized Circle Diagram Approach for Global Analysis of Transmission System Performance," *IEEE Trans. Power App. Syst.*, vol. PAS-103, no. 10, pp. 2881–2890, Oct. 1984.
- [13] I. Hiskens and B. Chakrabarti, "Direct Calculation of Reactive Power Limit Points," *Int. J. Elect. Power Energy Syst.*, vol. 18, no. 2, pp. 121–129, 1996.
- [14] Reactive Reserve Working Group under the auspices of Technical Studies Subcommittee of the Western Electricity Coordinating Council, "Guide to WECC/NERC Planning Standards I.D: Voltage Support and Reactive Power," Mar. 30, 2006.
- [15] W. Rosehart, C. Roman, and A. Schellenberg, "Optimal Power Flow with Complementarity Constraints," *IEEE Trans. Power Syst.*, vol. 20, no. 2, pp. 813–822, May 2005.
- [16] R. Avalos, C. Canizares, F. Milano, and A. Conejo, "Equivalency of Continuation and Optimization Methods to Determine Saddle-Node and Limit-Induced Bifurcations in Power Systems," *IEEE Trans. Circuits Syst. I, Reg. Papers*, vol. 56, no. 1, pp. 210–223, Jan. 2009.
- [17] D. Molzahn, B. Lesieutre, and C. DeMarco, "A Sufficient Condition for Power Flow Insolvability With Applications to Voltage Stability Margins," *IEEE Trans. Power Syst.*, vol. 28, no. 3, pp. 2592–2601, 2013.
- [18] R. Jabr, "Exploiting Sparsity in SDP Relaxations of the OPF Problem," *IEEE Trans. Power Syst.*, vol. 27, no. 2, pp. 1138–1139, May 2012.
- [19] D. Molzahn, J. Holzer, B. Lesieutre, and C. DeMarco, "Implementation of a Large-Scale Optimal Power Flow Solver Based on Semidefinite Programming," *IEEE Trans. Power Syst.*, vol. 28, no. 4, pp. 3987–3998, 2013.
- [20] D. Molzahn, V. Dawar, B. Lesieutre, and C. DeMarco, "Sufficient Conditions for Power Flow Insolvability Considering Reactive Power Limited Generators with Applications to Voltage Stability Margins," in *IREP Symp. Bulk Power Syst. Dynam. Control - IX. Optimiz., Secur. Control Emerg. Power Grid*, Aug. 25-30 2013.
- [21] S. Low, "Convex Relaxation of Optimal Power Flow: Parts I & II," *IEEE Trans. Control Network Syst.*, vol. 1, no. 1, pp. 15–27, Mar. 2014.
- [22] J. Jarjis and F. D. Galiana, "Analysis and Characterization of Security Regions in Power Systems, Part I: Load Flow Feasibility Conditions in Power Systems," McGill University, DOE/ET/29108–T1-Pt.1, Mar. 1980.
- [23] M. Ilic, "Network Theoretic Conditions for Existence and Uniqueness of Steady State Solutions to Electric Power Circuits," in *IEEE Int. Symp. Circuits Syst. (ISCAS)*, vol. 6, May 1992, pp. 2821–2828 vol.6.
- [24] F. Dörfler and F. Bullo, "Novel Insights into Lossless AC and DC Power Flow," in *2013 IEEE Power Eng. Soc. General Meeting*, Jul. 2013.
- [25] M. Ebrahimpour and J. Dorsey, "A Test for the Existence of Solutions in Ill-Conditioned Power Systems," in *IEEE Southeastcon*, Apr. 1991, pp. 444–448.
- [26] T. Overbye, "A Power Flow Measure for Unsolvable Cases," *IEEE Trans. Power Syst.*, vol. 9, no. 3, pp. 1359–1365, Aug. 1994.
- [27] —, "Computation of a Practical Method to Restore Power Flow Solvability," *IEEE Trans. Power Syst.*, vol. 10, no. 1, pp. 280–287, Feb. 1995.
- [28] V. Donde, V. Lopez, B. Lesieutre, A. Pinar, C. Yang, and J. Meza, "Severe Multiple Contingency Screening in Electric Power Systems," *IEEE Trans. Power Syst.*, vol. 23, no. 2, pp. 406–417, May 2008.
- [29] D. Molzahn, B. Lesieutre, and C. DeMarco, "Approximate Representation of ZIP Loads in a Semidefinite Relaxation of the OPF Problem," *IEEE Trans. Power Syst.*, vol. 29, no. 4, pp. 1864–1865, Jul. 2014.
- [30] J. Lavaei and S. Low, "Zero Duality Gap in Optimal Power Flow Problem," *IEEE Trans. Power Syst.*, vol. 27, no. 1, pp. 92–107, Feb. 2012.
- [31] J. Löfberg, "YALMIP: A Toolbox for Modeling and Optimization in MATLAB," in *IEEE Int. Symp. Compu. Aided Control Syst. Des.*, 2004, pp. 284–289.
- [32] S. Drewes, "Mixed Integer Second Order Cone Programming," Ph.D. Dissertation, Technische Universität Darmstadt, 2009.
- [33] L. Gan and S. Low, "Convex Relaxations and Linear Approximation for Optimal Power Flow in Multiphase Radial Networks," in *18th Power Syst. Comput. Conf. (PSCC)*, Aug. 2014.
- [34] M. Baran and F. Wu, "Optimal Capacitor Placement on Radial Distribution Systems," *IEEE Trans. Power Del.*, vol. 4, no. 1, pp. 725–734, Jan. 1989.
- [35] B. Lesieutre and I. Hiskens, "Convexity of the Set of Feasible Injections and Revenue Adequacy in FTR Markets," *IEEE Trans. Power Syst.*, vol. 20, no. 4, pp. 1790–1798, Nov. 2005.
- [36] Univ. Washington Power Syst. Archive, <http://www.ee.washington.edu/research/pstca/>.
- [37] Univ. Edinburgh Power Syst. Archive, "GB Network," <http://www.maths.ed.ac.uk/optenergy/NetworkData/fullGB/>.
- [38] R. Zimmerman, C. Murillo-Sánchez, and R. Thomas, "MATPOWER: Steady-State Operations, Planning, and Analysis Tools for Power Systems Research and Education," *IEEE Trans. Power Syst.*, no. 99, pp. 1–8, 2011.
- [39] S. Fliscounakis, P. Panciatici, F. Capitanescu, and L. Wehenkel, "Contingency Ranking with Respect to Overloads in Very Large Power Systems Taking into Account Uncertainty, Preventive and Corrective Actions," *IEEE Trans. Power Syst.*, vol. 28, no. 4, pp. 4909–4917, 2013.
- [40] D. Molzahn, C. Jozs, I. Hiskens, and P. Panciatici, "Solution of Optimal Power Flow Problems using Moment Relaxations Augmented with Objective Function Penalization," *IEEE 54th Ann. Conf. Decis. Control (CDC)*, Dec. 2015.